Climate Warming related strengthening of the tropical hydrological cycle

Matthias Zahn[1] & Richard P. Allan[2]

[1]*Environmental Systems Science Centre, University of Reading, 3 Earley Gate, Reading, Berkshire, RG6 6AL, UK.*

[2]*Department of Meteorology, University of Reading, Berkshire, Reading, United Kingdom*

Movements of moisture laden air constitute the atmospheric part of the hydrological cycle and play a major role in the distribution of moisture around the globe[1,2]. Future changes in the tropical hydrological cycle may alter the distribution of available fresh water regionally through altered moisture transport properties and precipitation minus evaporation patterns[3,4]. In this study we use high time and space resolution climate model simulations of a global climate change scenario to demonstrate enhanced moisture transport across the boundary between the dry regions of descending air into the moist regimes of ascending air motion. We found the low level inward and the mid level outward moisture transports of the convective regions in the tropics increase in a simulated anthropogenically warmed climate as compared to a simulated 20th century atmosphere, indicating an intensification of the hydrological cycle. Since an increase of inward transport exceeds the increase of outward transport the resulting budget is positive, meaning that more water is projected to converge in the moist tropics. The intensification is found to be due to the higher amount of water in the atmosphere, while the contribution of weakening wind counteracts this response marginally.

In addition to previous studies[5–7] we here investigate the changing statistical properties of the vertical profile of the moisture transport and for the first time (???) demonstrate the importance of the substantial outflow of moisture from the moist tropics at mid-levels.

The main component of the meridional atmospheric circulation in the tropics is the Hadley Cell, with equator-ward air movements and associated moisture transports at the lower levels. On average air along the Inter Tropical Convergence Zone (ITCZ) ascends and, at mid-levels, diverges and transports are directed pole-ward. Whether the tropical circulation or its components have intensified or weakened in the past decades has been discussed recently[8–11] and it has been subject to scientific studies how it may behave in a warmed future climate[5–7].

Contrary to these studies[5–7] mainly applying low resolution temporally averaged data we here calculate moisture transports in the present and an assumed future atmosphere based on homogeneous data high in spatial and temporal detail. Therefore we calculated the transports into ascending regions gained from mean fields of vertical wind (Ω), abbreviated ASC_m hereafter, constituting the well known pattern of the ITCZ, as well as into instantaneous ascending regions (ASC_i). In doing the latter we resolve much better individual convective cells rather than just using mean bands of ascending regions roughly spanning along the whole equator. We compared time slices of a simulated atmosphere generated by the model ECHAM5[12,13] valid for the end of the 21st century, 2069-2099, (C21), and for the 20th century (1959-1989, referred to as C20 hereafter). C20 was driven by observed Greenhouse Gas concentrations, C21 by assumptions for a possibly anthropogenically warmed future atmosphere[14] of the SRES A1B Intergovernmental

Panel of Climate Change (IPCC) scenario[15].

Both ways of defining the convective regions (ASC_m and ASC_i) result in an increase of accumulated overall inward transport as well as in an increase of the accumulated overall outward transport of moisture (table1). The difference of these numbers in C21 and C20 is statistically significantly different from zero at the 99.5 % level according to a t-test based on the instantaneous values of all time steps. Although the increase of inward and outward directed transports counteract the projected increase in the budget also is statistically significantly different from zero at the 99.5 % level.

Contrary to the idealised view on the Hadley Circulation the air flow is not directed towards the convective regions at all boundary segments at all times in the instantaneous wind fields. Rather inward and outward transport have a similar vertical shape (Supplementary Fig. 6), which is determined by the vertical distribution of moisture in the atmosphere. A weaker outward than inward transport at lower levels, and, vice versa, a stronger outward than inward transport at mid levels, results in the expected shape of the mean vertical profile of transports along the boundary of ascending (ASC) and descending regions (DESC) (Fig. 1). The vertical mean profile in all experiments and in re-analysis based comparison data from ERA-interim[16,17] is dominated by a maximum of inward transports at the lower levels, but a considerable outward one (negative values) is visible as well above a certain reversal level (RL).

Based on the vertical profile we have separated the transports below the reversal level and above, and calculated time series of the vertically aggregated yearly mean transports into ASC (positive values) below and of the the vertically aggregated yearly mean transport out of ASC (negative values) above the reversal level in each of the experiments (Fig. 2). Like the total transports, both the lower level inward as well as the mid level outward transport are projected to strengthen considerably in a warmed future. The change again is statistically significantly different from zero at 99.5% and results in an accelerated hydrological cycle. The percentage increase of the outward transport above RL is more than twice as large as the inward transport below RL ($MT_{out} \approx 38\%/MT_{in} \approx 17\%$) in both experiments, thus modifying simplistic views on precipitation change like e.g. in[18], who assume precipitation of the moist tropics to change at the same rate as lower level inward transport increases. The higher percentage increase in the outward moisture transport can be explained from theoretical considerations: following the Clausius Clapeyron equation humidity values at the higher (and thus colder) levels experience a higher percentage change than the lower[19], which is in line with our data (Supplementary Fig. 12).

Despite the increasing outward transports, a statistically significant increase is found for the budget ($MT_{in} - MT_{out}$), which, assuming a negligible increase in total atmospheric water storage, determines the change of precipitation in the tropics. Thus, in line with previous studies[20–23], tropical precipitation increases following our data.

Additionally to a strengthening of the hydrological cycle from C20 towards C21, we also found an acceleration of the strengthening. Significant changes were not found for C20, in accordance with simulations by ERA-interim[16,17], but there is a statistically significant trend over the 30 year C21 period (99.5% level, 97.5% for the ASC_m budget).

Previous studies[20–22] have not only suggested an increase in the mean tropical precipitation as a response to a warmed atmosphere, but especially a response in the higher percentiles of the distribution of precipitation events[24–26], commonly referred to as extreme events. To supply water for these events mass transport must also have increased in the upper percentiles. We here estimated the percentiles for the transports based on the approximately 45000 values at each of the model time steps of C20 and C21 into ASC_i at each level (Supplementary Fig. 9(a) and Fig. 9(b)), and their change over the projected century of warming in Supplementary Fig. 9(c). We find the most pronounced change in the highest percentiles of the low level inward transport and of the mid-level outward transport (compare large gaps between green and red line, which denotes the same 2% interval as green and blue line, respectively). The amount of increase of the strongest inward transport events (increase of 99%tile is $0.01629 kg * s^{-1} * m^{-1}$) is not counteracted by the same amount of outward transport (increase of 99%tile is $-0.00183 kg * s^{-1} * m^{-1}$), which is in the order of ten times smaller. While there is a near linear increase of the 20%-80% percentiles, the upper and lower end percentiles of moisture transport events increase much stronger (Supplementary Fig. 10). Thus, in order to maintain the atmospheric moisture capacity, the increased atmospheric moisture input must be precipitated out in more intense extreme events.

The moisture transports depend on two measures, the wind vectors and the atmospheric water content. Consequently, changes in the transport are provoked by changes in either of these two measures. In line with the Clausius-Clapeyron equation[18,27], precipitable water has increased with warming throughout the atmosphere over all percentiles (Fig. 3(a)) from C20 to C21. While the relative increase is stronger in the upper atmosphere (Supplementary Fig. 12), the absolute amount of change is strongest at low levels, and decreases with height.

The situation is different for the wind. The ’effective wind’, a measure for the wind circulation strength independent from the actual level thickness[10], is projected to weaken at the lower levels of inward flow (Fig. 3(b)). At the mid levels a strengthening as well as a reduction of the wind contribution was found for the outflow. We conclude the projected increase of the strength of the hydrological cycle is caused by higher humidity rather than circulation strength.

The major part of the moisture is transported into ASC meridionally, following the Hadley Circulation. Although some events occasionally are directed the opposite way we find this Hadley pattern is represented generally very well at our southern boundaries. The situation at the norther boundary is more complex and median (50% percentile) is only slightly above 0.

Generally the southern boundary inward transports dominate those at the northern boundary by far, which may be due to the distribution of land-sea mass across the globe. Northern boundaries of ASC are much more likely to be situated over land than the southern ones. Over land, however, air carries lower amounts of water due to lower supply by evaporation and circulation patterns are much more influenced by orography and thus much more complex, e.g. directed northward against the main flow even at low levels. Over the course of a warming 21st century a widening of the percentiles of lower level inward and outward transport events are observed at both, the northern as well as the southern boundary. However the median only increases (by almost a quarter) at the southern boundary, whereas the already low value at the northern boundary gets even smaller. Thus the domination of the southern boundary for the moisture transports increases.

There may be an influence of the latitude ASC is located at since regions closer to the equator are normally warmer and thus air can carry more moisture here, allowing for larger moisture transports. We found large changes of the frequency a particular grid box belongs to ASC in the two experiments, ASC_i and ASC_m, with a change of less the $2\ \%$ in few areas only (white in Fig. 4(a)). Along the equatorial oceans spans an area of increasing likelihood to belonging to ASC, indicating more convection. North and south are some areas, especially in ASC_m (Fig. 4(b)), with less frequent upward vertical wind velocity. This suggests a narrowing of the ITCZ in these regions as opposed to findings by[28], shifting their borders to warmer latitudes enhancing the transports in addition to the already warming atmosphere.

There are major areas of less frequent ascending air movement over the Indonesian islands, the up-draft region of the Walker Circulation. Associated with the Walker Circulation is a down-draft of air masses over the tropical Pacific. Our findings suggest a weakening of the Walker Circulation, with less frequent convection in its up-drafting and more frequent convection in its down-drafting branch in a warmed atmosphere, in line with a previous study[9] and with a weakening of zonal tropical circulations with warming in general[5].

Although changes are qualitatively similar for both experiments, numbers are more distinct in ASC_m. The different changes are explained by a non Gaussian distribution of vertical wind speeds. Grid cells, which are frequented by strong convective cells (with high upward Ω) only at a few time steps are rarely assigned to ASC_i, but will be assigned to ASC_m when the upward Ω at these few situations is high enough to out-range the otherwise low intensity down-draft situations

Table 1: Average of inward (MTin) and outward (MTout) moisture transport in C20 and C21. To calculate the inward/outward transport, transports at all boundary segments are used which are directed inward/outward of ASC.

	average $MTin[kg * s^{-1} * m^{-1}]$	average MTout $[kg * s^{-1} * m^{-1}]$	average budget $[kg * s^{-1} * m^{-1}]$
$C20_m$	67.6788	-62.3744	5.30434
$C21_m$	81.8478	-75.9407	5.90717
$C20_i$	72.2925	-64.1567	8.13585
$C21_i$	87.9224	-78.8052	9.11721

in the averaging. One may speculate that some extremely intensive convective cells from more intense tropical storms in a warmed atmosphere[29] may cause the differently pronounced change between ASC_i and ASC_m.

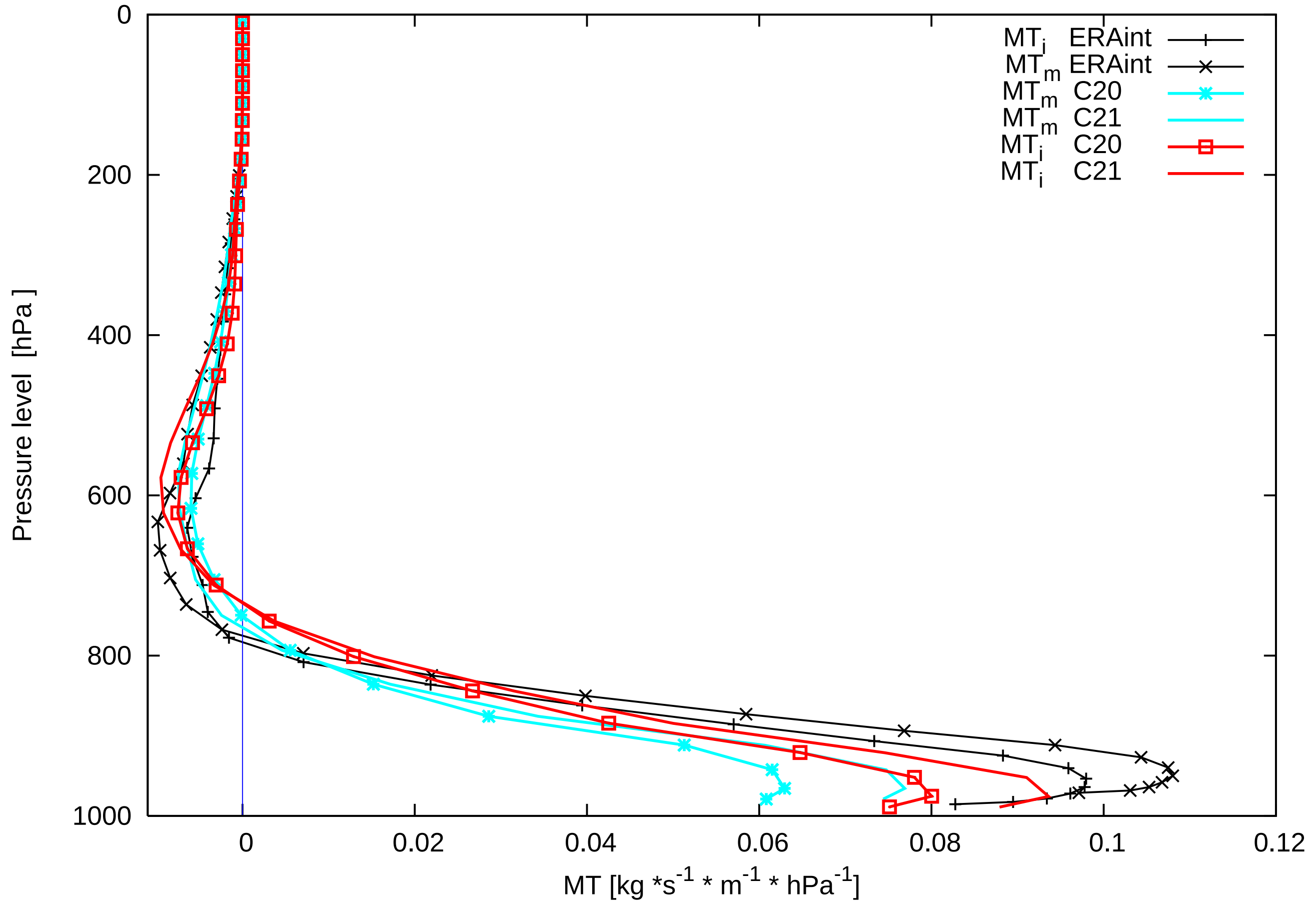

Figure 1: **Vertical profiles of horizontal moisture transports.** Magnitude of horizontal net moisture transport per hPa along ASC/DESC boundary from ECHAM5 and ERA-interim[16,17] into ASC_i and ASC_m. Positive/negative values denote net transports into/out of ASC. Symbols denote locations of mean pressure and mean transports. Unit of transport is mass of water [kg] per time [s] and area [$hPa * m$]. Note that the vertical unit of the area is given in pressure [hPa].

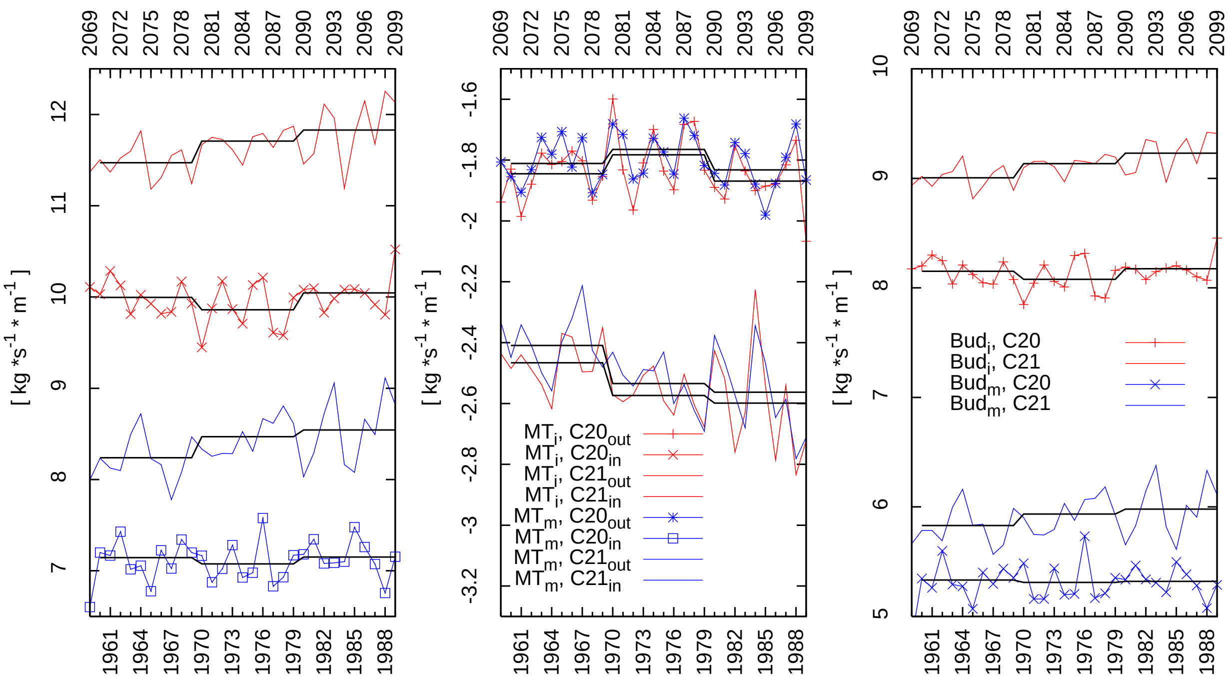

(a) MT_{in} (b) MT_{out} (c) Budget

Figure 2: **Temporal evolution of moisture transport into the ascending region.** Times series of mean yearly moisture transports over ASC/DESC boundary below (a) and above (b) the reversal level. (c) time series of the yearly mean budget. C21 years refer to upper x-axis, C20 years refer to lower x-axis. Plain lines indicate C21 values, lines with symbols refer to C20 values. Flags for (a) are given in (b). Black lines indicate decadal means (1st, 2nd and 3rd decade of each data set), respectively.

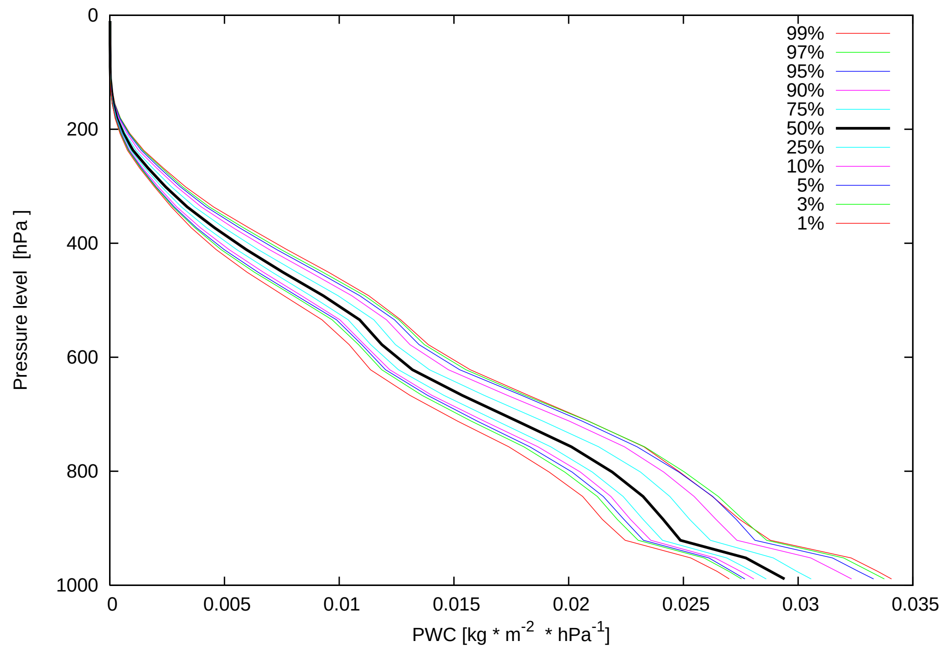

(a) PWC

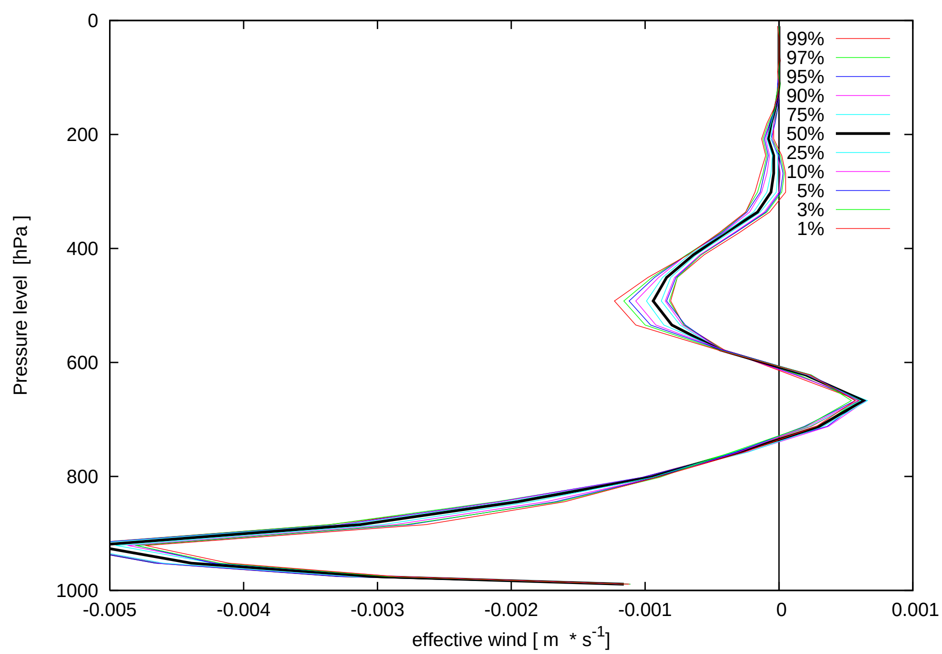

(b) effective wind

Figure 3: **Changes of percentiles of precipitable water and of effective wind along boundary of convective regions.** (a) Vertical profile of difference in the percentiles of precipitable water and (b) vertical profile of difference in the percentiles of the effective wind (C21 - C20, respectively). Here, effective wind is the mean wind directed towards ASC at a given level, weighted by the water content at the same level relative to the total column water content, following the definition of [10].

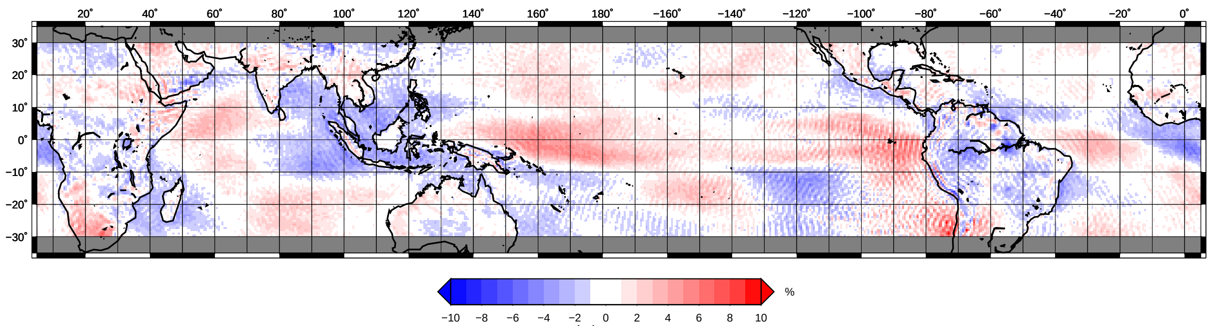

(a) ASC_i

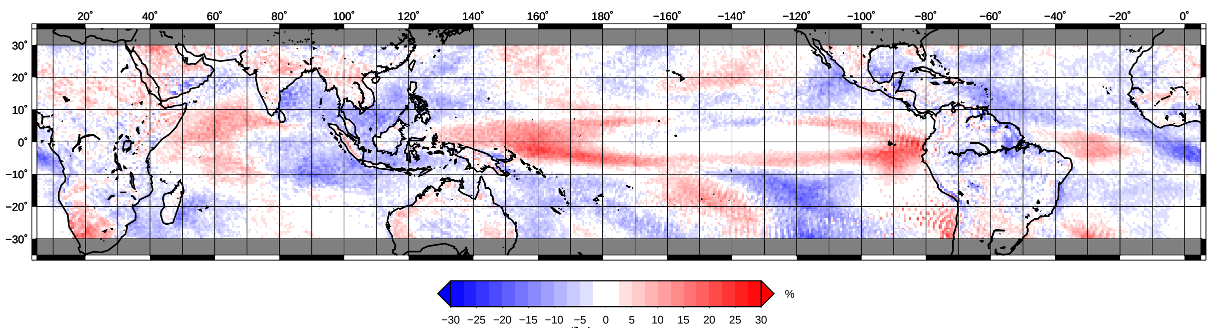

(b) ASC_m

Figure 4: **Changing frequency of the ascending regions.** (a) Change of percentage of time steps a grid box belongs to ASC from the instantaneous vertical wind (ASC_i), C21 - C20. (b) Change of percentage a grid box belongs to ASC when derived from the monthly mean vertical wind (ASC_m), C21 - C20. Red indicates a box belongs to ASC more frequently, blue means it belongs to ASC less frequently. Note the different scale of the colour bar.

Methods

We used T213 ($0.5°$) horizontal resolution ECHAM5 model[12] data at 31 vertical levels driven by different Greenhouse Gas (GHG) Concentrations for two 31 years time slices, 1959-1989 (C20) and 2069-2099 (C21). The simulations are of the time slice type forced with boundary data from a coupled climate simulation with the same model at T63 resolution. The C20 GHG concentrations are the observed ones, the C21 were delivered by the A1B scenario[15] of the Fourth Assessment Report (AR4) of the Intergovernmental Panel of Climate Change (IPCC). We used vertical (Ω) and horizontal (U,V) wind vectors, specific humidity and surface air pressure for all 31 model levels (from the surface up $0\ hPa$) in a two-staged approach for calculating the moisture transports:

- in model results of both, C20 and C21, we identified regions of ascending and of descending Ω and defined the boundary separating both
- in model results of both, C20 and C21, we identified the U, V, humidity and pressure at each level along the boundary and calculated the moisture transport

Definition of Ascending and Descending regions and of the boundary in between

At each grid cell in the tropical region between $-30°$ and $30°$ latitude the sum of the vertical wind motion Ω of the lower and middle part of the atmosphere, the lowest 21 model levels corresponding to a height of up to approximately $450hPa$ was estimated. Before summing up, the vertical motion representative for each level was weighted by the thickness of each level. Grid boxes with an upwards directed overall Ω were assigned to the ascending region (ASC), else, if

$\Omega = 0$ or directed downwards they were assigned to the descending regions (DESC). The boundary over which moisture transports are estimated is defined as the line separating ASC and DESC. If ASC or DESC is cut by the $-30°$ or $30°$ latitude line, an artificial boundary is drawn along this latitude to avoid 'open' regions.

ASC and DESC were estimated based on monthly mean values as well as on instantaneous values representative for the 180 seconds of the calculation time step in the ECHAM5 model. Example fields of both are shown in Supplementary Fig. 5. Please note that while the mean ASC/DESC masks reflect the general ITCZ pattern with ASC stretching along the the equator, the instantaneous field exhibits a much more complex pattern of convective cells and down-draft regions.

Calculation of moisture transports

At each time step t the moisture transport is calculated across all the n_b boundary segments b between ASC and DESC (green lines in Fig. 4) at each of the n_l vertical model levels l by multiplying the perpendicular wind vector (WP) with the precipitable water content (PWC), respectively. The resulting total moisture transport (MT) per time step then reads:

$$MT_t = \sum_{b}^{n_b} \sum_{l}^{n_l} WP_{bl} \cdot PWC_{bl} \tag{1}$$

Since applying mean wind speeds and mean PWC has proven to be insufficient previously[17], the calculations were only conducted using instantaneous variables. We should not that in the C21 output the fields at three time steps, at 18 Jan 2077 12:00 , at 18 Jan 2077 18:00 and at 31 Aug 2079 18:00 were corrupt. They were replaced by the data at 18 Jan 2077 06:00, at 19 Jan 2077 00:00 and at 31 Aug 2079 12:00, respectively.

1. Trenberth, K. E., Smith, L., Qian, T., Dai, A. & Fasullo, J. Estimates of the global water budget and its annual cycle using observational and model data. *J. Hydrometeor* **8**, 758769 (2007).

2. Bengtsson, L. The global atmospheric water cycle. *Environ. Res. Lett.* **5** (2010).

3. Allen, M. R. & Ingram, W. J. Constraints on future changes in climate and the hydrologic cycle. *Nature* **419**, 224–232 (2002).

4. Trenberth, K. E., Dai, A., Rasmussen, R. M. & Parsons, D. B. The changing character of precipitation. *Bull. Amer. Met. Soc.* **84**, 1205–1217 (2003).

5. Vecchi, G. A. & Soden, B. J. Global warming and the weakening of the tropical circulation. *J. Climate* **20**, 4316–4340 (2007).

6. Seager, R., Naik, N. & Vecchi, G. A. Thermodynamic and dynamic mechanisms for large-scale changes in the hydrological cycle in response to global warming. *Journal of Climate* **23**, 4651–4668 (2010). URL

http://journals.ametsoc.org/doi/abs/10.1175/2010JCLI3655.1.

http://journals.ametsoc.org/doi/pdf/10.1175/2010JCLI3655.1.

7. Chou, C. & Chen, C.-A. Depth of convection and the weakening of tropical circulation in global warming. *J. Climate* **23**, 30193030 (2010).

8. Mitas, C. M. & Clement, A. Has the Hadley cell been strengthening in recent decades? *Geophys. Res. Lett.* **32** (2005).

9. Vecchi, G. A. *et al.* Weakening of tropical pacific atmospheric circulation due to anthropogenic forcing. *Nature* **441**, 73–76 (2006). URL http://dx.doi.org/10.1038/nature04744.

10. Sohn, B. J. & Park, S.-C. Strengthened tropical circulations in past three decades inferred from water vapor transport. *J. Geophys. Res.* **11** (2010).

11. Young, I. R., Zieger, S. & Babanin, A. V. Global trends in wind speed and wave height. *Science* **332**, 451–455 (2011). URL http://www.sciencemag.org/content/332/6028/451.abstract.

http://www.sciencemag.org/content/332/6028/451.full.pdf.

12. Roeckner *et al.* The atmospheric general circulation model ECHAM 5. PART I: Model description. *MPI-Report No 349* (2003).

13. Roeckner, E. *et al.* Sensitivity of simulated climate to horizontal and vertical resolution in the echam5 atmosphere model. *J. Climate* **19**, 37713791 (2006).

14. Meehl, G. *et al.* *Climate Change 2007: The Physical Science Basis*, chap. Global Climate Projections (Cambridge University Press, Cambridge, United Kingdom and New York, NY, USA, 2007).

15. Nakicenovic, N. & Swart, R. (eds.) *IPCC Special Report on Emissions Scenarios* (Cambridge Univ. Press, 2000).

16. Dee, D. P. *et al.* The ERA-interim reanalysis: configuration and performance of the data assimilation system. *Quarterly Journal of the Royal Meteorological Society* **137**, 553–597 (2011). URL `http://dx.doi.org/10.1002/qj.828`.

17. Zahn, M. & Allan, R. P. Changes in water vapor transports of the ascending branch of the tropical circulation. *J. Geophys. Res.* **116** (2011).

18. Held, I. M. & Soden, B. J. Robust responses of the hydrological cycle to global warming. *J. Climate.* **19**, 5686–5699 (2006).

19. Allan, R. The role of water vapour in earths energy flows. *Surveys in Geophysics* 1–8. URL `http://dx.doi.org/10.1007/s10712-011-9157-8`. 10.1007/s10712-011-9157-8.

20. Wentz, F. J., Ricciardulli, L., Hilburn, K. & Mears, C. How much more rain will global warming bring? *Science* **317**, 233 – 235 (2007).

21. Stephens, G. L. & Ellis, T. D. Controls of global-mean precipitation increases in global warming GCM experiments. *J. Climate* **21**, 61416155 (2008).

22. Allan, R. P., Soden, B. J., John, V. O., Ingram, W. & Good, P. Current changes in tropical precipitation. *Environmental Research Letters* **5**, 025205 (2010). URL `http://stacks.iop.org/1748-9326/5/i=2/a=025205`.

23. Liu, C. & Allan, R. P. Multi-satellite observed responses of precipitation and its extremes to interannual climate variability. *J. Geophys. Res.* **in press.** (2011).

24. Kharin, V. V., Zwiers, F. W., Zhang, X. & Hegerl, G. C. Changes in temperature and precipitation extremes in the IPCC ensemble of global coupled model simulations. *J. Climate* **20**, 14191444 (2007).

25. Lenderink, G. & van Meijgaard, E. Increase in hourly precipitation extremes beyond expectations from temperature changes. *Nature Geoscience* **1** (2008).

26. Allan, R. P. & Soden, B. J. Atmospheric warming and the amplification of precipitation extremes. *Science* **321**, 1481–1484 (2008).

27. Wentz, F. J. & Schabel, M. Precise climate monitoring using complementary satellite data sets. *Nature* **403**, 414–416 (2000).

28. Lu, J., Vecchi, G. A. & Reichler, T. Expansion of the Hadley cell under global warming. *Geophys. Res. Lett.* **34** (2007).

29. Knutson, T. R. *et al.* Tropical cyclones and climate change. *Nature Geoscience* **3**, 157 – 163 (2010).

30. John, V. O. & Soden, B. J. Temperature and humidity biases in global climate models and their impact on climate feedbacks. *Geophys. Res. Lett.* **34** (2007).

31. Zahn, M. & von Storch, H. Decreased frequency of north atlantic polar lows associated with future climate warming. *Nature* 309–312 (2010).

32. Christensen, J. *et al.* *Climate Change 2007: The Physical Science Basis*, chap. Regional Climate Projections (Cambridge University Press, Cambridge, United Kingdom and New York, NY, USA, 2007).

Acknowledgements The simulations were performed with the ECHAM5 model developed at the Max-Planck Institute for Meteorology, Germany, at HLRN (Norddeutscher Verbund für Hoch und Höchstleistungsrechnen). We are thankful to Noel Keenlyside and Kevin Hodges for help with these data and for discussions. M.Z. was funded by the NERC PREPARE project, NE/G015708/1.

Contributions M.Z. and R.A. developed the ideas presented. M.Z. wrote the manuscript and did the technical work for this study.

Correspondence Correspondence and requests for materials should be addressed to M.Z. (email: m.zahn@reading.ac.uk).

1 Supplementary Online Material

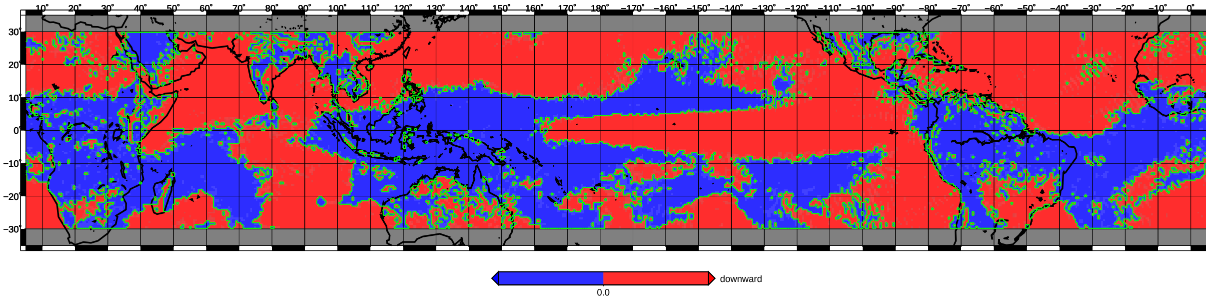

(a) ASC_m Mar 1965

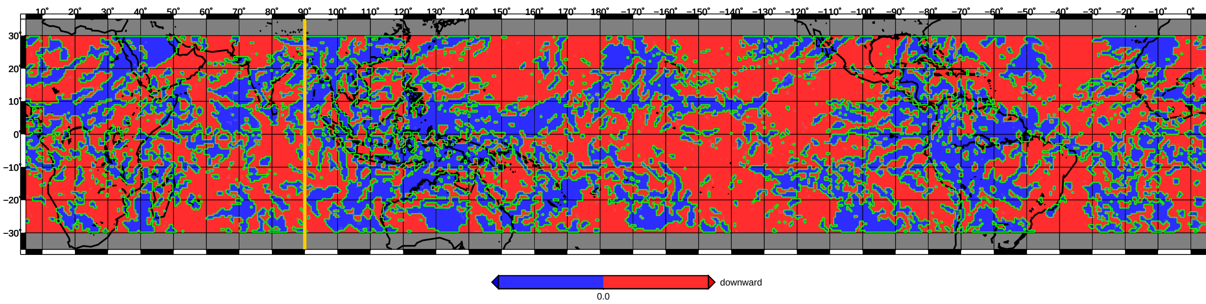

(b) ASC_i 22 Mar 1965, 6:00am

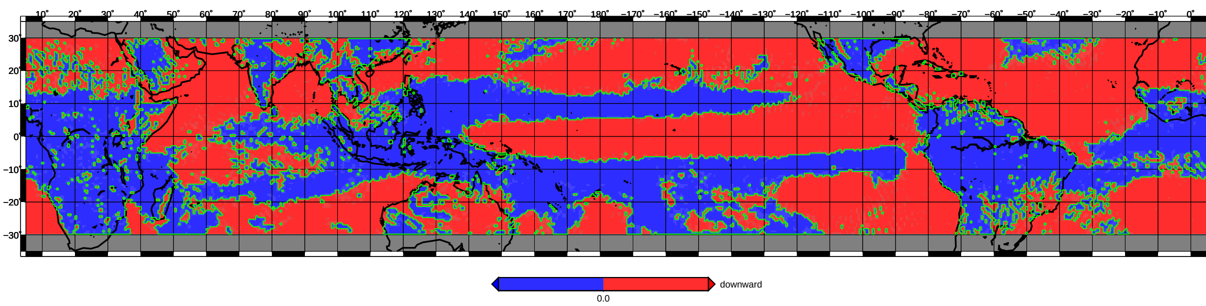

(c) ASC_m Mar 2075

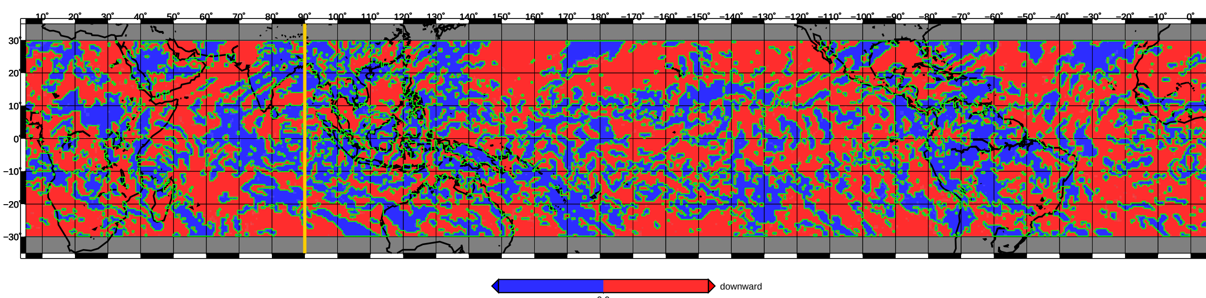

(d) ASC_i 22 Mar 2075, 6:00am

Figure 5: **Example fields of $\mathrm{ASC_i}$ and of $\mathrm{ASC_m}$ in C20 and C21.** Distribution of ascending and descending regions from ECHAM5, red denotes down-draft, blue denotes up-draft, green is the boundary line across which fluxes are calculated. (a) valid March 1965, (b) valid 22 March 1965, 6:00am, (c) valid March 2075 and (d) valid 22 March 2075, 6:00am.

BIAS ECHAM5 ERA-interim

All our experiments based on ECHAM5 share a similar profile as those from a previous study applying re-analysis data[17], which consider observations to reconstruct the actual synoptic weather situation using a numerical model including data assimilation. However biases exist between our model data and the re-analysis based results. For instance although the vertical profiles qualitatively are similar, there are differences in the exact amount of transports at most levels. Also, the exact amount of net moisture transport per year is different, but the statistical property of no trend in 20th century are shared by the C20 ECHAM5 and ERA-interim based study. Biases between model and re-analysis/observation data and also between data from different models are a common feature often described before[30,31] and are referred to in the IPCC-AR4 report[14,32]. They may originate from different physics and different sub grid scale parametrisations in various models. However, despite the biases, climate models have widely been used to study the details of climate change.

In our re-analysis based study[17] we found a slightly positive, but no statistically significant trend of moisture transports, neither inward nor outward the ascending regions in the tropics over the period 1989 through 2008. Inward and outward transports from those data have been calculated (analogous to table1) as $56.8/-48.1 kg * s^{-1} * m^{-1}$ for ASC_m and $63.6/-54.4 kg * s^{-1} * m^{-1}$ for ASC_i and are in the order of $10 kg * s^{-1} * m^{-1}$ smaller than in ECHAM5, resulting in higher budgets of $8.7/9.2 kg * s^{-1} * m^{-1}$ for ASC_m/ASC_i . Nevertheless transports from ECHAM5 and from ERA-interim re-analysis share the same statistical properties, a positive, but insignificant trend.

The reason for the higher budget in the ERA-interim data becomes evident from Supplementary Fig. 6. While the vertical profile of the C20 inward transport resembles that of ERA-interim well, the difference denoting the lower outward transport in ERA-interim, and thus the higher budget, is more obvious. Apart from the different physics and parametrisations in ECHAM5 its higher resolution may play a role in the bias. Please note that adding the left and right hand-side of this bell-shaped Supplementary Fig. 6 results in the mean vertical profile of the moisture transports as given in Fig. 1.

To investigate closer the origin of the bias we plotted the vertical profiles of available precipitable water per level along the border between ASC and DESC and of the meridional wind components at the northern and southern boundary, marking the Hadley Cell's wind components in Supplementary Fig. 7. We found the humidity in ECHAM5 to be much higher, but the meridional wind at the lower level to be weaker compared to ERA-interim. So, two biases neutralise each other in this case, at least to some extent.

We here investigate the statistical properties of the change of tropical moisture transports, which in the re-analysis and C20 model based data are similar. We thus conclude that the latter are suitable for our investigations.

Percentiles of vertical moisture transports

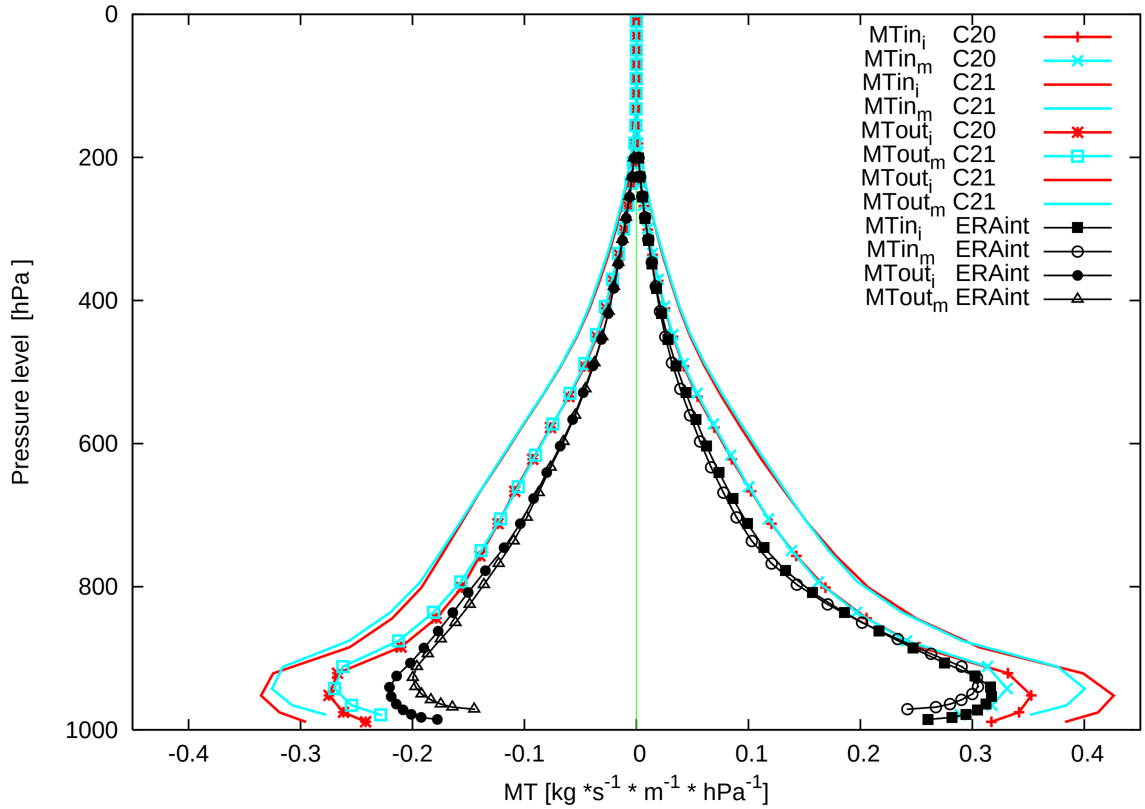

Figure 6: **Vertical profile of inward and outward transport of moisture.** Curves on the left/right hand-side show the average vertical profile of outward/inward transport of moisture per height (negative/positive values) for the total period of the different experiments. Curves for C20 are denoted by lines with points, those for C21 are denoted by plain lines.

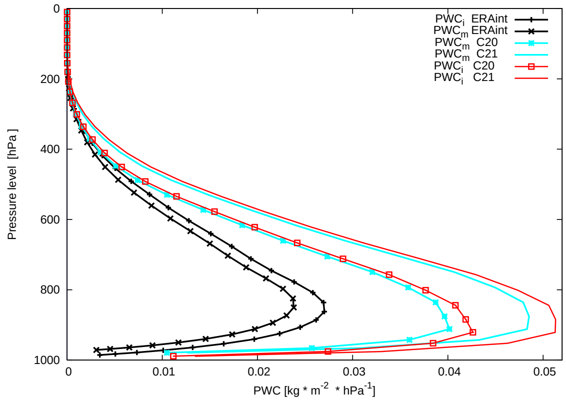

(a) PWC

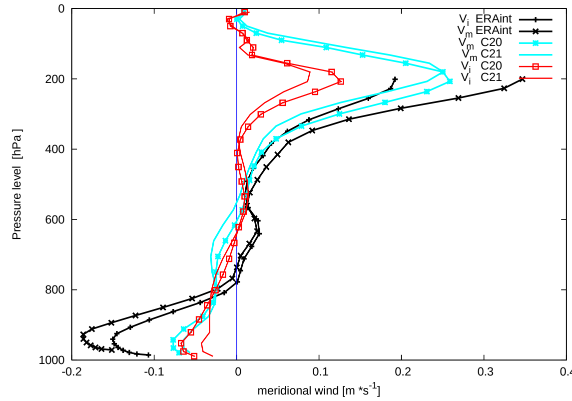

(b) meridional wind along northern boundary

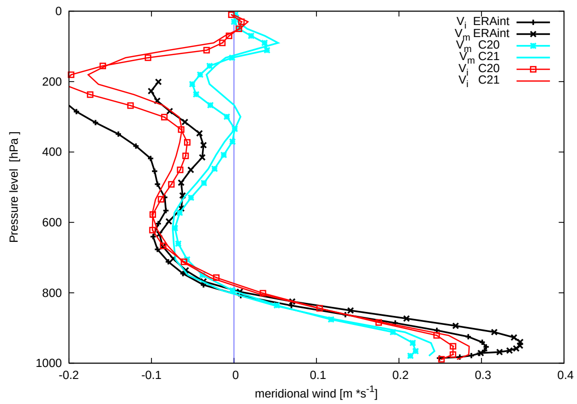

(c) meridional wind along southern boundary

Figure 7: **Precipitable water along boundary of ASC and meridional wind of the Hadley Circulation along northern/southern boundary of ASC.** (a) Averaged amount of water in a $m^2 \times hPa$ box along boundary of ASC and level's average wind at its (b) northern and (c) southern boundary. Numbers derived for the C20 time slice (lines with symbols) and for the C21 time slice (plain lines). Black lines denote ERA-interim, for ASC_m and ASC_i. Blue lines denote ECHAM5 data for ASC_m and red lines denote ECHAM5 data using ASC_i. Curves for C20 are denoted by lines with points, those for C21 are denoted by plain lines.

The most commonly used statistical value is the arithmetic mean, herein referred to as mean. However the mean normally delivers only an insufficient picture of a quantity's distribution. To include changes at the upper and lower end of the distribution of the vertical moisture transports we here additionally showed their percentiles at a given level. The x-percentile is a threshold value above which $x\%$ of the observations (in our case simulated quasi instantaneous moisture transports) are situated. We here used for each experiment the mean moisture transport over the boundary between ASC and DESC at each simulated time step. Thus percentiles are calculated based on populations of more than 45000 observations ($31[years] * 365[days/year] * 4[observations/day] \approx 45000[observations]$).

Mean and percentiles of moisture transports at the northern and southern boundaries and in C20 and C21 are shown in Supplementary Fig. 8. In this case the mean value is virtually similar to the median, the 50% percentile. It becomes evident that the mean and median do reflect a moisture transport profile following the idealised Hadley Cell pattern, with inward transport at low levels and outward transport at mid levels. However it becomes also evident, that this profile is not valid in many of the instantaneous situations. In fact, it can be directed the opposite sense in many cases, especially at the low levels. The situation at the northern boundary is farther apart from the idealised situations as it may be influenced stronger by more complex small scale situations influences by land air interaction.

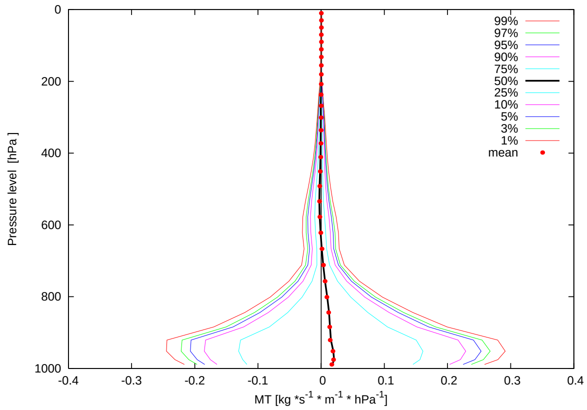

(a) at northern boundary, C20

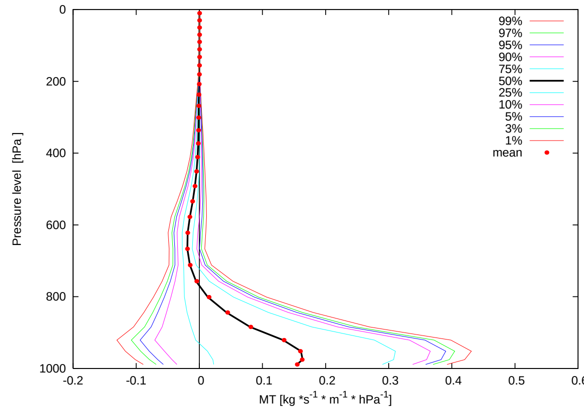

(b) at southern boundary, C20

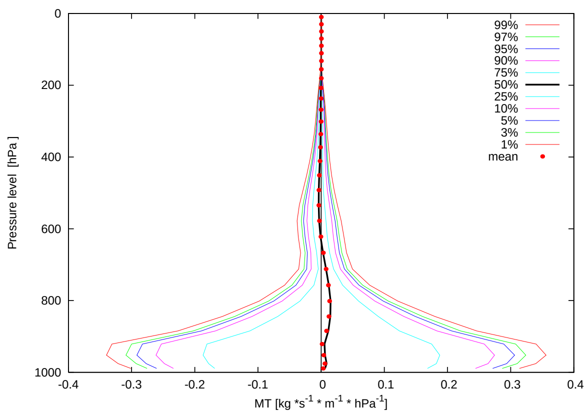

(c) at northern boundary, C21

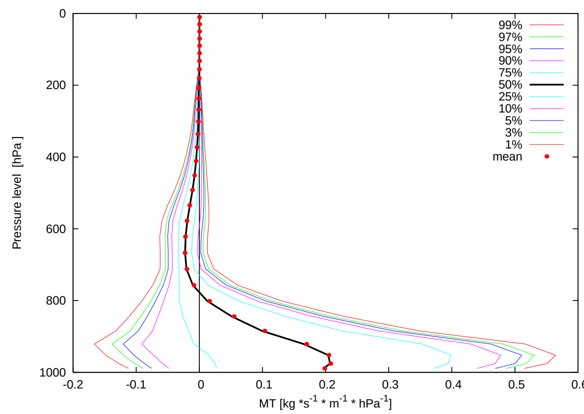

(d) at southern boundary, C21

Figure 8: **Vertical structure of percentiles of moisture transports at northern and southern boundaries of $\mathbf{ASC_i}$.** (a) At the northern boundary in C20. (c) At the northern boundary in C21. (b) At the southern boundary in C20. (d) At the southern boundary in C21. Also given is the mean transport per hPa, respectively.

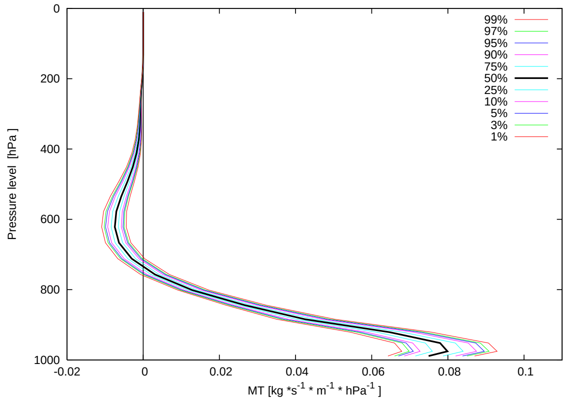

(a) C20

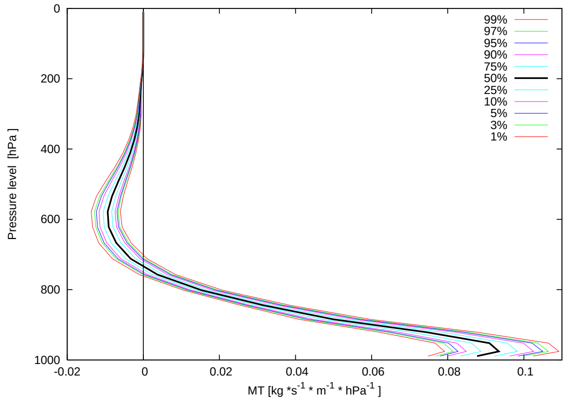

(b) C21

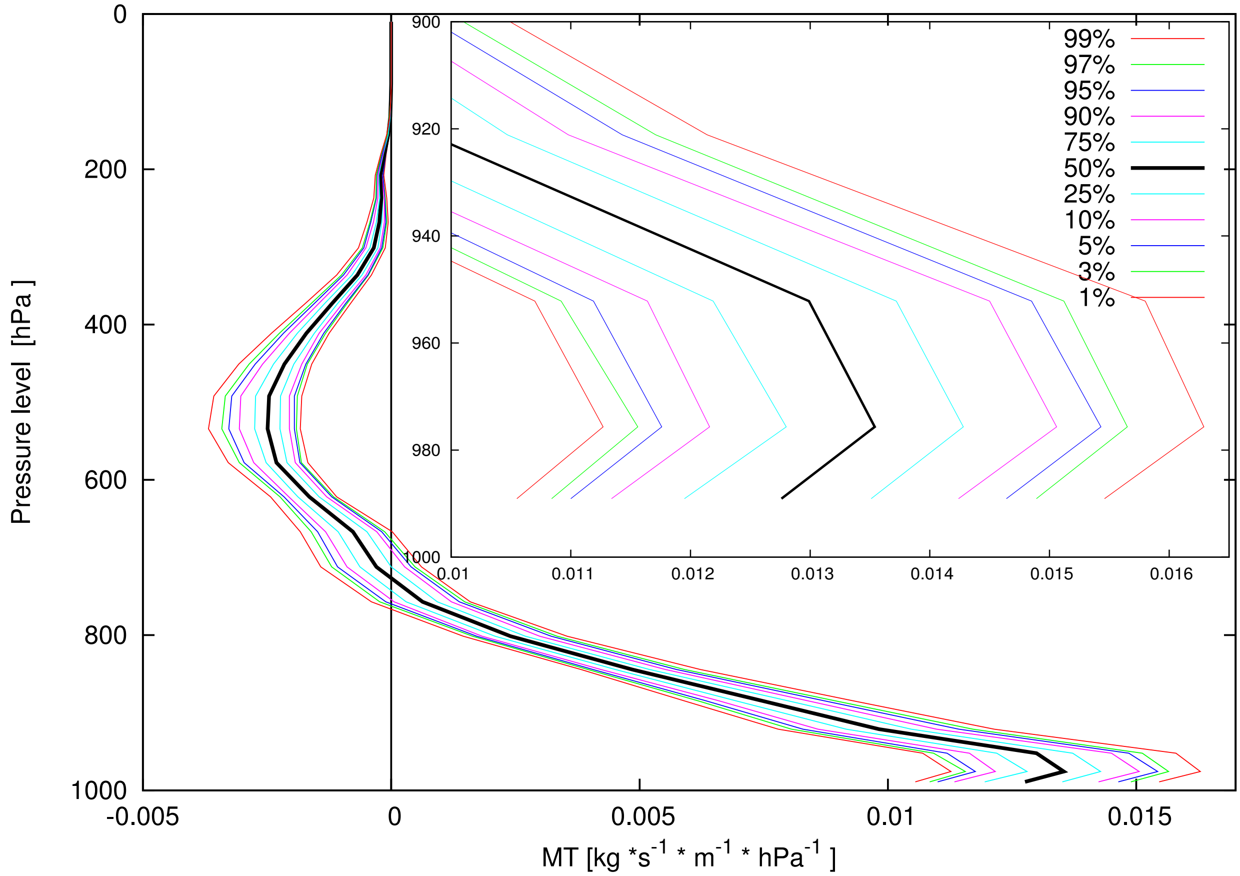

(c) C21 - C20

(c)

Figure 9: **Vertical structure of percentiles of moisture transports.** Vertical structure of percentiles of moisture transports (a) for C20 and (b) for C21. (c) Vertical profile of the difference between both, C21 - C20. Lower right corner is enlarged.

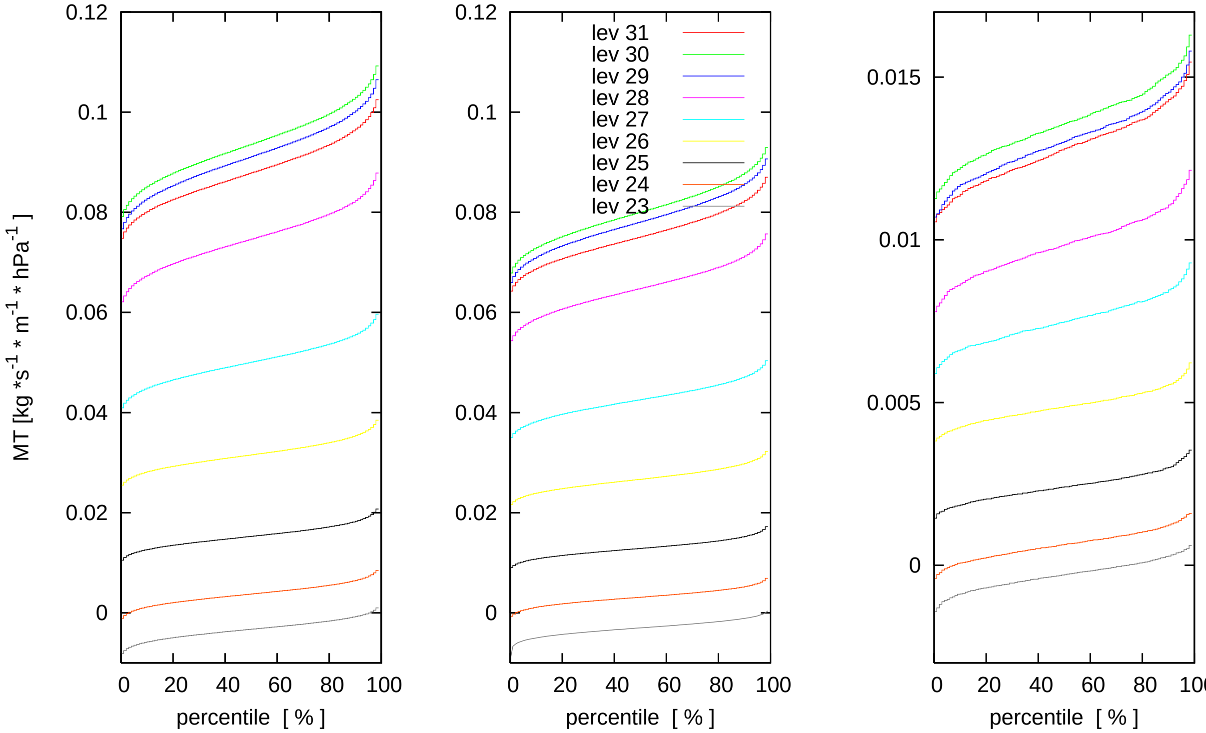

(a) C21

(b) C20

(c) C21 - C20

Figure 10: **Percentiles of moisture transports at lower levels.** (a)Percentiles of moisture transports at lower levels for C21, (b) percentiles of moisture transports at lower levels for C20 and (c) difference of percentiles of moisture transports at lower levels, C21 - C20. Colours of levels in (b) are also valid for (a) and (c).

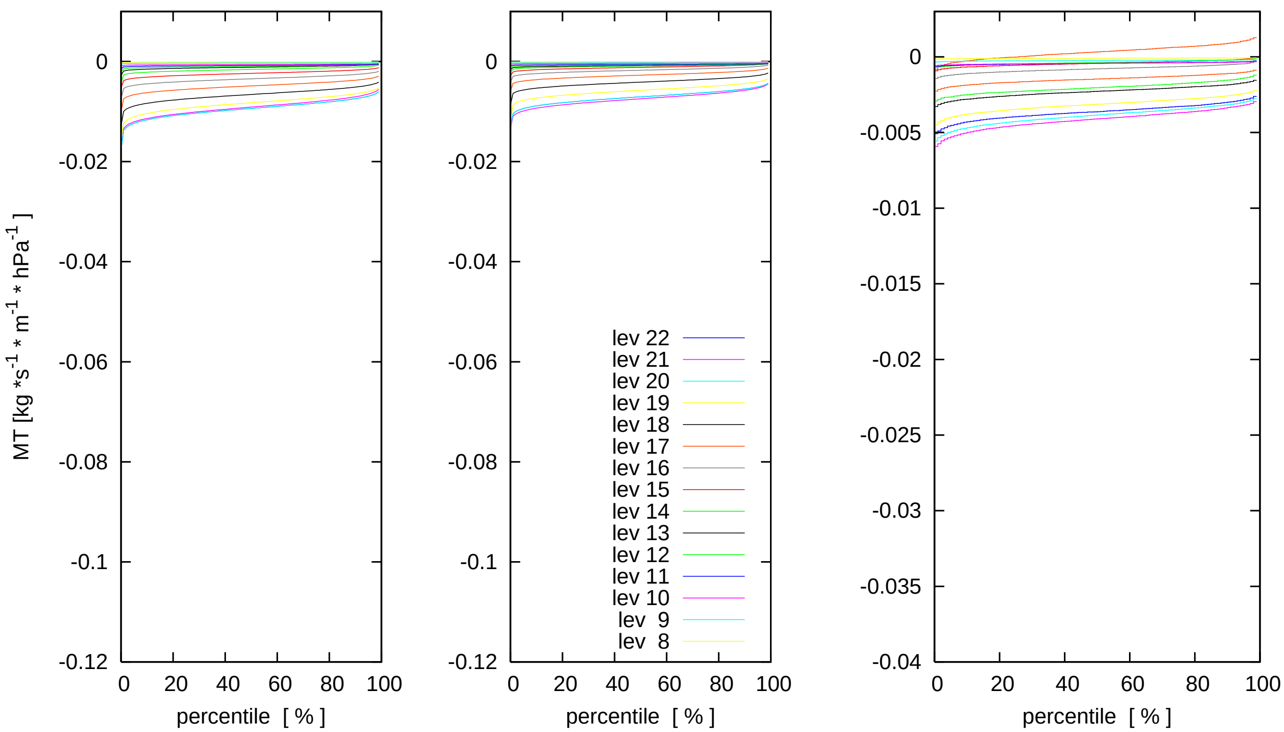

(a) C21 (b) C20 (c) $C21 - C20$

Figure 11: **Percentiles of moisture transports at mid levels.** (a) Percentiles of moisture transports at mid levels for C21, (b) percentiles of moisture transports at mid levels for C20 and (c) difference of percentiles of moisture transports at mid levels, C21 - C20. Colours of levels in (b) are also valid for (a) and (c).

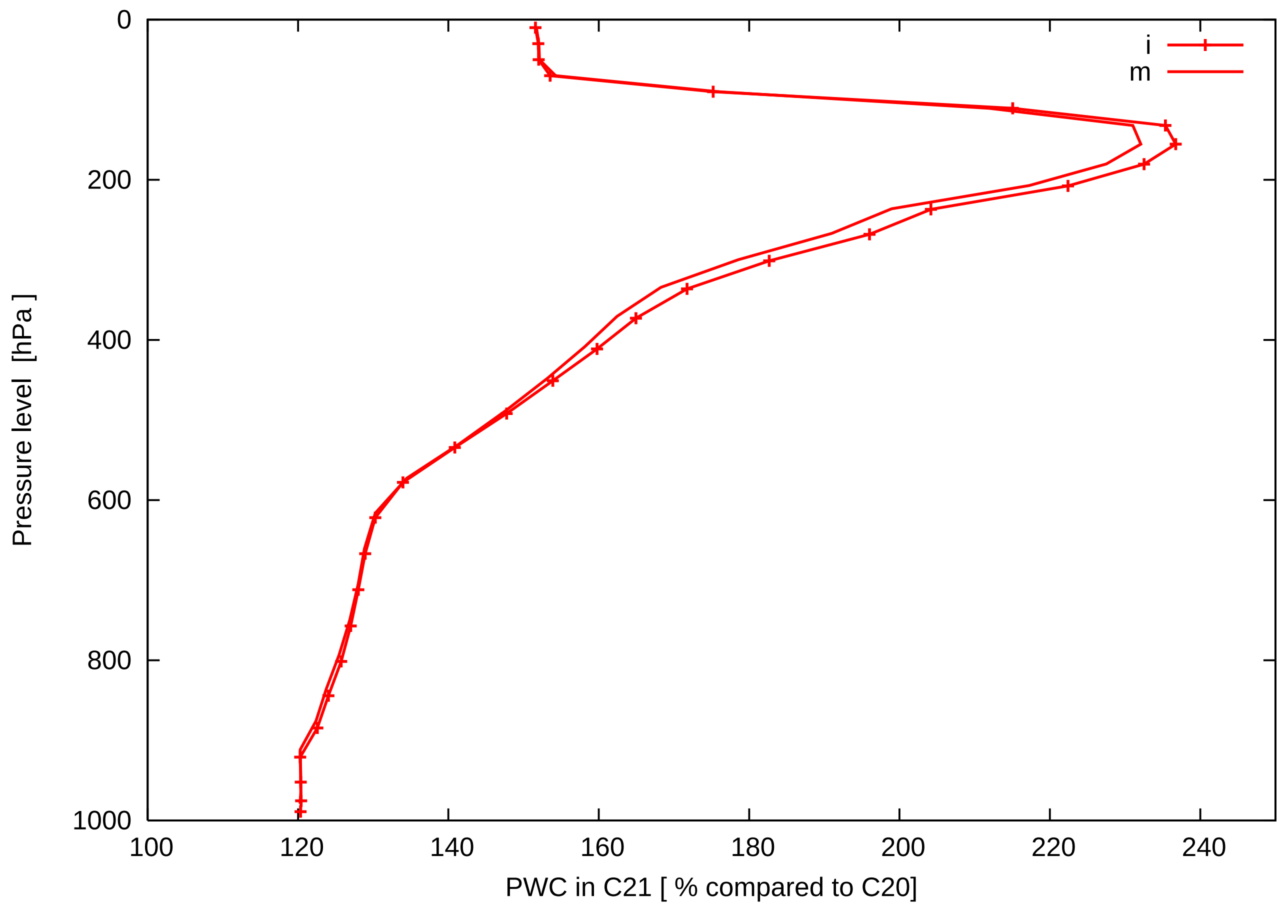

Figure 12: **PWC along boundaries in C21 relative to C20.** Percentage of precipitable water content along ASC/DESC boundary of ASC_i and ASC_m in C21 relative to C20. Unit of transport is mass of water [kg] per time [s] and area [$hPa * m$]. Note that the vertical unit of the area is given in pressure [hPa].